Dalton Transactions

PAPER

View Article Online
View Journal | View Issue

Cite this: *Dalton Trans.*, 2015, **44**, 13359

Molecular Pac-Man and Tacos: layered Cu(II) cages from ligands with high binding site concentrations†

Cecelia McDonald,[a] David W. Williams,[b] Priyanka Comar,[c] Simon J. Coles,[d] Tony D. Keene,[d] Mateusz B. Pitak,[d] Euan K. Brechin[c] and Leigh F. Jones*[a,b]

Received 17th April 2015,
Accepted 23rd June 2015

DOI: 10.1039/c5dt01463h

www.rsc.org/dalton

The *in situ* formation and subsequent Cu(II) ligation of the polydentate pro-ligands *o*-[(*E*)-(2-hydroxy-3-methoxyphenyl)methylideneamino]benzohydroxamic acid (L_1H_3), *o*-[(*E*)-(2-hydroxy-3-methoxy-5-bromophenyl)methylideneamino]benzohydroxamic acid (L_2H_3) and *o*-[(*E*)-(2-hydroxyphenyl)methylideneamino]benzohydroxamic acid (L_3H_3), leads to the self-assembly of the cages $[Cu^{II}_{10}(L_1)_4(2\text{-aph})_2(H_2O)_2](ClO_4)_4\cdot 5MeOH$ (**1**), $[Cu^{II}_{14}(L_1)_8(MeOH)_{2.5}(H_2O)_{7.5}](NO_3)_4\cdot 3MeOH\cdot 7H_2O$ (**2**), $[Cu^{II}_{14}(L_2)_8(MeOH)_4(H_2O)_6](NO_3)_4\cdot 6H_2O$ (**3**), $[Cu^{II}_{14}(L_3)_8(MeOH)_6(H_2O)_2](NO_3)_4\cdot 4MeOH\cdot 8H_2O$ (**4**) and $[Cu^{II}_{30}O(OH)_4(OMe)_2(L_1)_{16}(MeOH)_4(H_2O)_2](ClO_4)_4\cdot 2MeOH\cdot 30H_2O$ (**5**). Each member comprises a highly unusual topology derived from off-set, stacked, near planar layers of polynuclear subunits connected through long Cu(II)–O contacts. The exact topology observed is dependent on the specific reaction conditions and methodologies employed. Dc magnetic susceptibility studies on **1**, **2**, **4** and **5** reveals strong antiferromagnetic exchange between the Cu(II) centres in all siblings. We also present the 1D coordination polymer $\{[Cu^{II}(L_4)]\cdot H_2O\}_n$ (**6**) comprising the pseudo macrocyclic ligand [[2-[(*E*)-(2-hydroxy-3-methoxyphenyl)methyleneamino]benzoyl]amino]ethanimidate (L_4H_2), which is formed upon the incorporation of an MeCN unit at the hydroxamate group of precursor ligand L_1H_3.

Introduction

The strategic formation and rapid metal complexation of pre-designed ligands from their 'simpler' organic precursors has become an important synthetic tool towards otherwise unattainable metal–ligand architectures of varying complexities. This specific process is commonly described as subcomponent self-assembly[1] and is a subtle extension upon the field of template-directed synthesis.[2] Although other examples are known in the literature,[3] the Nitschke group have notably demonstrated that the Schiff base condensation of various aldehyde and amine moieties, driven by reversible C=N and M–N bond formation,[1,2] are versatile precursors towards the preparation of numerous host–guest metal container complexes of varying topologies.[4]

Indeed, the process of producing a ligand '*in situ*' in the presence of a metal ion has also benefitted the field of molecular magnetism, where a number of polymetallic transition metal cages have been produced (*e.g.* $[Mn_{14}]$,[5] $[Fe_{10}]$,[6] and $[Dy_8]$,[7]), albeit *via* a more serendipitous route. In a similar vein we describe here the Cu(II) ligation of the polydentate pro-ligands *o*-[(*E*)-(2-hydroxy-3-methoxyphenyl)methylideneamino]-benzohydroxamic acid (L_1H_3), *o*-[(*E*)-(2-hydroxy-3-methoxy-5-bromophenyl)methylideneamino]benzohydroxamic acid (L_2H_3) and *o*-[(*E*)-(2-hydroxyphenyl)methylideneamino]benzohydroxamic acid (L_3H_3; Scheme 1) – formed by the imine condensation of 2-(amino)phenylhydroxamic acid and either 2-hydroxy-3-methoxybenzaldehyde (for L_1H_3), 5-bromo-2-hydroxy-3-methoxybenzaldehyde (for L_2H_3) or 2-hydroxybenzaldehyde (for L_3H_3). Here we combine two of our most recently (and successfully) employed ligands, hydroxamic acids[8] and phenolic imines,[9] to form moieties comprising multiple metal binding sites in order to encourage polynuclear cage formation.

Results and discussion

To this end we present the synthesis, structural and magnetic characterisation of the cages: $[Cu^{II}_{10}(L_1)_4(2\text{-aph})_2(H_2O)_2](ClO_4)_4\cdot 5MeOH$ (where 2-aphH_2 is 2-(amino)phenylhydroxamic

[a]*School of Chemistry, NUI Galway, University Road, Galway, Ireland*
[b]*School of Chemistry, Bangor University, Bangor, Wales LL57 2DG, UK. E-mail: leigh.jones@bangor.ac.uk; Tel: +44(0)1248-38-2391*
[c]*EaStCHEM School of Chemistry, Joseph Black Building, University of Edinburgh, West Mains Road, Edinburgh, Scotland EH9 3JJ, UK*
[d]*UK National Crystallographic Service, Chemistry, Faculty of Natural and Environmental Sciences, University of Southampton, England, SO17 1BJ, UK*
† Electronic supplementary information (ESI) available. CCDC 1055293–1055298. For ESI and crystallographic data in CIF or other electronic format see DOI: 10.1039/c5dt01463h

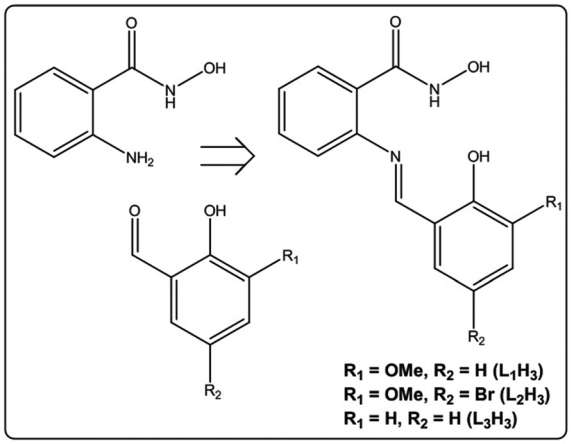

Scheme 1 General structure (right) and precursors (left) of the ligands L_xH_3 (x = 1–3) utilised in this work.

acid) (**1**), $[Cu(II)_{14}(L_1)_8(MeOH)_{2.5}(H_2O)_{7.5}](NO_3)_4{\cdot}3MeOH{\cdot}7H_2O$ (**2**), $[Cu(II)_{14}(L_2)_8(MeOH)_4(H_2O)_6](NO_3)_4{\cdot}6H_2O$ (**3**), $[Cu(II)_{14}(L_3)_8(MeOH)_6(H_2O)_2](NO_3)_4{\cdot}4MeOH{\cdot}8H_2O$ (**4**) and $[Cu(II)_{30}O(OH)_4(OMe)_2(L_1)_{16}(MeOH)_4(H_2O)_2](ClO_4)_4{\cdot}2MeOH{\cdot}30H_2O$ (**5**). Pro-ligands L_1H_3, L_2H_3 and L_3H_3 are unknown in the literature in terms of their synthesis and subsequent complexation.

The decametallic complex $[Cu(II)_{10}(L_1)_4(2\text{-aph})_2(H_2O)_2](ClO_4)_4{\cdot}5MeOH$ (**1**) (Fig. 1) crystallises in the monoclinic $C2/c$ space group and was formed from a methanolic solution of $Cu(ClO_4)_2{\cdot}6H_2O$ and a 1 : 1 equimolar mixture of L_1H_3 precursors: 2-(amino)phenylhydroxamic acid and 2-hydroxy-3-methoxy-benzaldehyde (Scheme 1), in the presence of a suitable base (NaOH). All pertinent crystallographic data for **1** and siblings **2–4** are given in Table S1.† The crystal structure in **1** adds to a relatively small number of discrete decametallic Cu(II) assemblies[10] although a small number of wheel-like architectures are also known in the literature.[11]

The core in **1** comprises two near planar $\{Cu_5\}$ sheets linked in an off-set fashion by a combination of long Cu–O contacts (Cu5–O4 = 2.777 Å) and bridging O_{phen} atoms (O2 from L_1^{3-} ligands), resulting in its rather unusual taco-shaped arrangement (Fig. 1 and 2). The Cu(II) ion arrangement within each $\{Cu_5\}$ layer is best described as comprising three (distorted) edge-sharing triangles whose edges are spanned by a combination of 2 × L_1^{3-} moieties and a single 2-(amino)phenylhydroxamate (2-aph^{2-}) ligand- a precursor to the formation of L_1H_3. Despite varying the reaction conditions in **1**, the L_1^{3-}/2-aph^{2-} ligand combination is consistently produced, whereas complexes **2–4** each exclusively comprise our Schiff base ligands (L_1H_3, L_2H_3 or L_3H_3; *vide infra*). The four L_1^{3-} ligands in **1** exhibit remarkably high binding site concentrations represented by the $\eta^1{:}\eta^2{:}\eta^1{:}\eta^1{:}\eta^2{:}\eta^1$ μ_4- bonding mode, while the 2-aph^{2-} ligands display a $\eta^1{:}\eta^2{:}\eta^1{:}\eta^1$ μ_3- bridging motif. Metal centres Cu1, Cu3 and Cu4 (and symmetry equivalent, s.e.) possess distorted square based pyramidal geometries (τ = 0.36, 0.11 and 0.14 respectively), the latter two ions exhibiting long axial Cu–O contacts to the nearby ClO_4^- counter anions lying

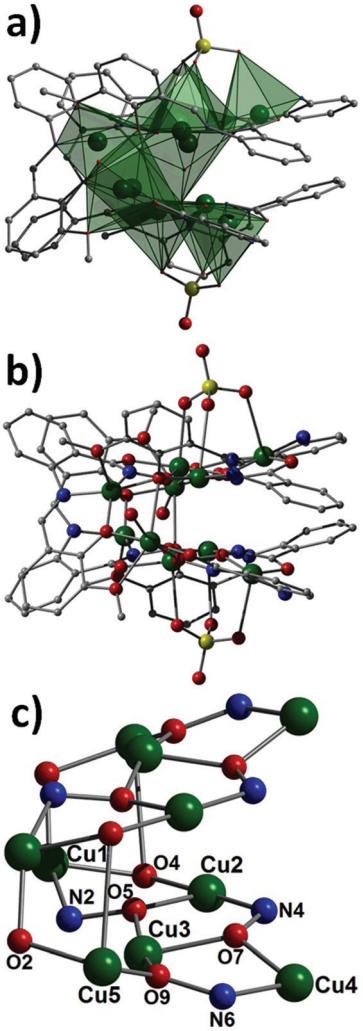

Fig. 1 Polyhedral (a) and standard (b) representation of the crystal structure in **1**. All hydrogen atoms have been omitted for clarity. (c) The inorganic core in **1**. Colour code (used throughout this work): green (Cu), red (O), blue (N), grey (C) and yellow (Cl).

above the $\{Cu_5\}$ planes in **1** (Cu3–O17 = 2.440 Å, Cu4–O18 = 2.794 Å). The Cu2 centre (and s.e.) is of distorted square planar geometry although the aforementioned perchlorate anions give rise an extremely long Cu–O contact at its axial site at a distance of 2.872 Å (Cu2–O19). The Cu5 centre (and s.e.) exhibits a Jahn–Teller distorted octahedral geometry thanks to two axially elongated Cu–O bonds (Cu5–O1 = 2.231 Å and Cu5–O4 = 2.777 Å), while a terminal H_2O ligand completes its coordination sphere (Cu5–O11 = 1.948 Å). Despite the close proximity of the $\{Cu_5\}$ units in **1**, no formal intramolecular π–π interactions are observed between their respective L_1^{3-} and 2-aph^{2-} aromatic rings. Two sets of symmetry equivalent perchlorate counter anions maintain electroneutrality in **1**, with one set directly 'bound' to the $\{Cu_{10}\}$ cage through the aforementioned long Cu–O contacts, while the second set lie further afield. The individual $\{Cu_{10}\}$ units in **1** pack in a brick-work motif along the *ab* plane of the unit cell. These sheets

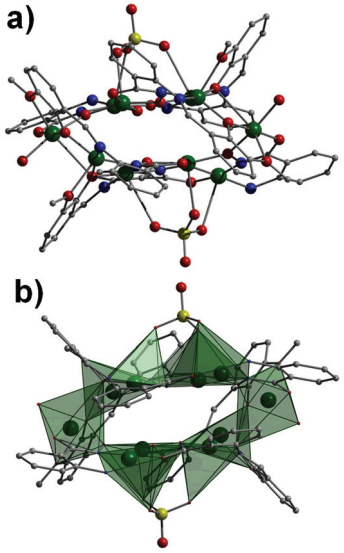

Fig. 2 Alternative perspective of **1**. All hydrogen atoms have been omitted for clarity.

then stack in parallel off-set rows along the *c* cell direction (Fig. 3).

The analogous complexes $[Cu(II)_{14}(L_1)_8(MeOH)_{2.5}(H_2O)_{7.5}](NO_3)_4{\cdot}3MeOH{\cdot}7H_2O$ (**2**), $[Cu(II)_{14}(L_2)_8(MeOH)_4(H_2O)_6](NO_3)_4{\cdot}6H_2O$ (**3**) and $[Cu(II)_{14}(L_3)_8(MeOH)_6(H_2O)_2](NO_3)_4{\cdot}4MeOH{\cdot}8H_2O$ (**4**) are readily obtained *via* the ambient reaction of cupric nitrate hexahydrate and L_xH_3 (x = 1 (**2**), x = 2 (**3**), x = 3 (**4**); made *in situ*) in MeOH and in the presence of a suitable base. It should also be noted that the structure in **2** can also be synthesised using microwave heating (see Experimental section for details). The homovalent $[Cu(II)_{14}]$ complexes **2–4** join an exclusive group of tetradecametallic copper clusters. However, all bar one of these members are mixed valence Cu(I/II),[12] while a sole mono-valent $[Cu(I)_{14}]$ cage was recently reported by Zhang and co-workers.[13]

Akin to the structure in **1**, complexes **2–4** have layered structures this time comprising the fusion of two $\{Cu_7\}$ units (Fig. 4 and Fig. S1 and S2†). The dark green crystals in **2–4** crystallise in the triclinic $P\bar{1}$ (**2**), monoclinic $C2/c$ (**3**) and $P2_1/c$ (**4**) space groups respectively, and their contrasting symmetries are manifested (in part) by the stacking arrangements of the $\{Cu_7\}$ units relative to one other. More specifically, the two heptanuclear moieties in **4** stack directly on top of one another in a pseudo superimposable fashion, while the two $\{Cu_7\}$ layers in **2** and **3** sit at approximate right angles to one another as highlighted in Fig. 5 and S2.† Apart from these obvious differences the three structures share many similarities and will be discussed in general terms from herein. The Cu(II) centres within each $\{Cu_7\}$ unit in **2–4** comprise two triangular arrays joined by a central cupric ion (Cu1 and Cu8 in **2**, Cu4 in both **3** and **4**) (Fig. S6†). The L_1^{3-} and L_2^{3-} ligands in **2** and **3** respectively, utilise an equal distribution of $\eta^1{:}\eta^2{:}\eta^1{:}\eta^1{:}\eta^2{:}\eta^1$ μ_4- and $\eta^1{:}\eta^2{:}\eta^1{:}\eta^1{:}\eta^1$ μ_3-bonding modes to construct their $\{Cu_7\}$ units. A combination of $\eta^1{:}\eta^2{:}\eta^1{:}\eta^1{:}\eta^2$ μ_4- and $\eta^1{:}\eta^2{:}\eta^1{:}\eta^1{:}\eta^1$ μ_3-bridging motifs are employed by the L_3^{3-} ligands in sibling complex **4** (Fig. 6). The $\{Cu_7\}$ planes in **2–4** are then connected by Jahn–Teller elongated axial Cu–O contacts to produce their final topologies (*i.e.* Cu2–O30 = 2.698 Å in **2**, Cu5B–O50 = 2.855 Å in **3** and Cu7–O1 = 2.718 Å in **4**) (Fig. 4). The majority of the Cu centres in **2–4** exhibit distorted square based pyramidal geome-

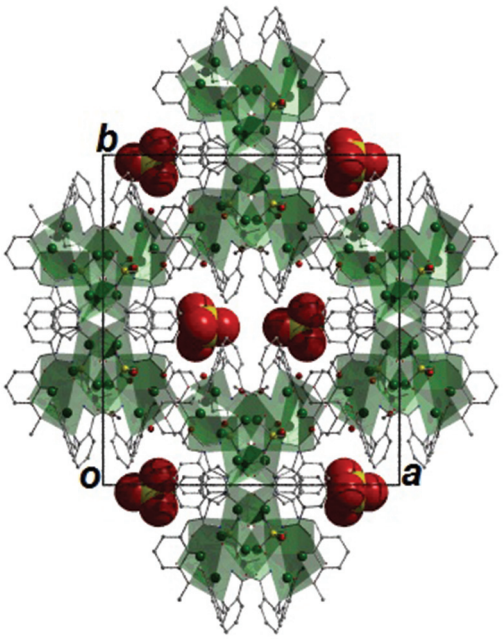

Fig. 3 Crystal packing in **1** as viewed along the *c* unit cell direction. Note: only the non-coordinated ClO_4^- counter anions are represented in space-fill mode. Hydrogen atoms have been omitted for clarity.

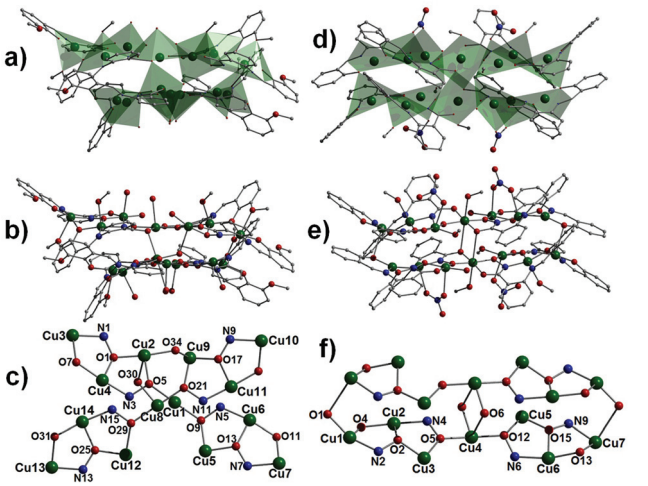

Fig. 4 Polyhedral and standard representations of the crystals in **2** (a and b respectively) and **4** (d and e respectively). All hydrogen atoms have been omitted for clarity. The NO_3^- counter anions in **2** were also omitted for clarity. (c) and (f) represent the inorganic cores in **2** and **4** respectively.

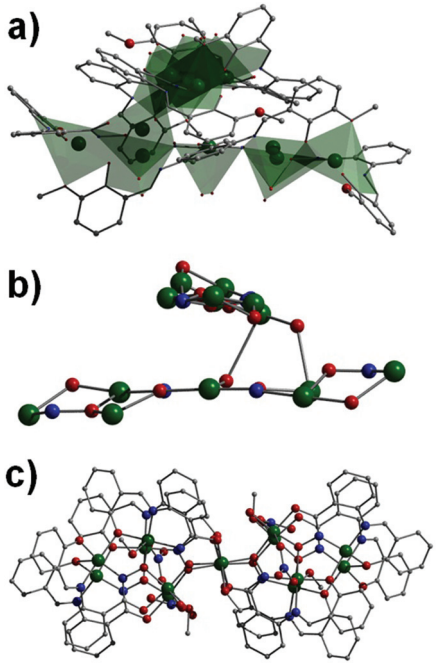

Fig. 5 The criss-cross orientation of the $\{Cu_7\}$ planes in **2** and **3** (a and b) as opposed to the pseudo superimposable stacking arrangement observed in **4** (c).

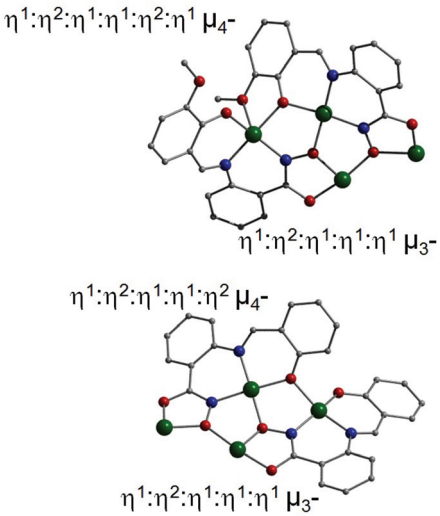

Fig. 6 The two different bonding modes exhibited by the L_1^{3-} ligands in **2** (top) and L_3^{3-} ligands in **4** (bottom). All hydrogen atoms have been omitted for clarity.

tries. The remaining metal centres in **2** exhibit distorted octahedral geometries (*i.e.* Cu2 and Cu9), while a single Cu(II) centre in **4** (Cu1 and s.e.) is of a distorted square planar geometry. Terminal methanol, water and/or NO_3^- moieties complete the coordination spheres at many of the Cu(II) centres in **2–4.**

Intramolecular interactions between terminally bound H_2O protons (H37B) and adjacent carbonyl O atoms (*e.g.* O6) are prevalent in the structure of **2** (O37(H37B)···O6 = 1.640 Å). Likewise, strong intermolecular hydrogen bonding interactions between unbound NO_3^- oxygen atoms (*e.g.* O47A) and juxtaposed terminally bound water protons (H42A) are also observed in **2** (O47A···H42A = 1.747 Å). The individual $\{Cu_{14}\}$ units in **2** arrange in superimposable rows along the *a* direction of the unit cell and pack along the *bc* plane in the familiar brickwork pattern (Fig. 7-left).

Intramolecular interactions are observed in **4** between metal bound methanol ligands with juxtaposed NO_3^- anions (*e.g.* O21(H21)···O18 = 2.062 Å) as well as unbound water molecules (O43(H43)···O47 = 2.213 Å). These interstitial waters of crystallisation sit in-between the $\{Cu_{14}\}$ units and effectively connect them to one another using extensive hydrogen bonding with their terminal MeOH, H_2O and NO_3^- ligands (*e.g.* O10···O40 = 2.544 Å and O8···O45 = 2.777 Å). The $\{Cu_{14}\}$ moieties in **4** arrange in superimposable rows along the *c* direction of the unit cell and exhibit weak inter-chain $\pi_{centroid}\cdots\pi_{centroid}$ interactions (*e.g.* [C43–C48]···[C50–C55] = 4.510 Å). These individual rows pack in the brickwork motif along the *ab* plane (Fig. 7-right), as also seen for **3** (Fig. S3†).

Solvothermal heating of a basic methanolic solution containing $Cu(ClO_4)_2{\cdot}6H_2O$ and the L_1H_3 precursors 2-(amino)-phenylhydroxamic acid and 2-hydroxy-3-methoxybenzaldehyde – a high temperature, high pressure repetition of the ambient reaction that produced complex **1** – affords the complex $[Cu_{30}O(OH)_4(OMe)_2(L_1)_{16}(MeOH)_4(H_2O)_2](ClO_4)_4{\cdot}2\text{-}MeOH{\cdot}30H_2O$ (**5**). Discounting the extremely large and numerous copper-chalcogenide[14] nanoclusters known in the literature (*e.g.* the staggering $[Cu_{136}S_{56}(SCH_2C_4H_3O)_{24}\text{-}(dpppt)_{10}]$ cage; where dpppt = 1,5-bis(diphenylphosphino)-pentane),[15] the architecture in $[Cu_{30}]$ (**5**) represents one of the largest O-donor Cu(II) cages known and is only smaller than the complexes $[K_4(\mu\text{-}MeOH)_4][Cu(II)_{36}(\mu_3\text{-}OH)_{32}(\mu\text{-}OR)_8Cl_6\text{-}(ndpa)_8(H_2O)_5\{KCl_6\}]$ (R is H or Me); H_3ndpa = (nitrilodipropionic)-

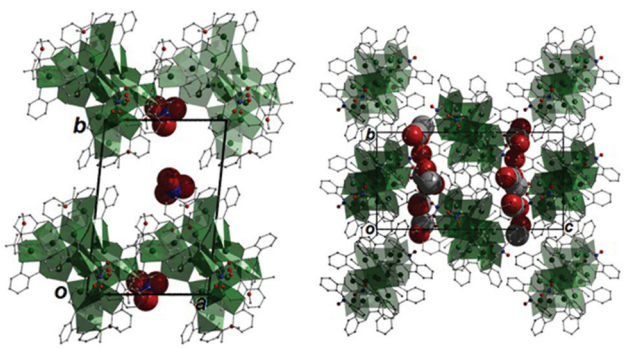

Fig. 7 (Left) Polyhedral packing diagram of **2** as viewed along the *c* unit cell axis. Only the non-coordinating NO_3^- anions are shown in the space–fill mode. (Right) Polyhedral representation of the packing in **4** as viewed along the *a* axis of the unit cell. MeOH solvents of crystallisation are represented using the space-fill mode.

acetic acid)[16] and $[Cu(II)_{44}(\mu_8\text{-}Br)_2(\mu_3\text{-}OH)_{36}(\mu\text{-}OH)_4(ntp)_{12}Br_8(H_2O)_{28}]Br_2{\cdot}81H_2O$ (where H_3ntp = aminopolycarboxylate nitrilotripropionic acid).[17]

Complex **5** crystallises in the triclinic $P\bar{1}$ space group and once more comprises a layered structure as observed in **1–4** (see Table S2† for details). More specifically, a central $\{Cu_{16}(O)(OH)_4(L_1)_8\}^{2+}$ unit (layer 2 in Fig. 8d) forms a platform which is sandwiched between two offset $\{Cu_7(OMe)(L_1)_4(MeOH)_2(H_2O)_x\}^+$ layers (x = 0 in layer 1; x = 2 in layer 3; Fig. 8d) to form the Pac-Man shaped $[Cu_{30}]$ superstructure (Fig. 8a and b). The central $\{Cu_{16}\}$ fragment may also be described as comprising two near planar $\{Cu_8\}$ sub-fragments which are connected by a centrally located distorted tetrahedral μ_4- bridging O^{2-} anion (O36; Fig. 8c). The metal centres within each $\{Cu_8\}$ moiety are held together *via* two μ-bridging OH^- ions (O22, O31, O45 and O57) alongside four L_1^{3-} ligands showing an equal distribution of $\eta^1{:}\eta^2{:}\eta^1{:}\eta^1{:}\eta^2{:}\eta^1$ μ_4- and $\eta^1{:}\eta^2{:}\eta^1{:}\eta^1{:}\eta^1$ μ_3-bonding modes (Fig. 9-left). This bonding mode combination is also employed by the four L_1^{3-} ligands that bridge the metal centres within each of the two bowl-shaped $\{Cu_7\}$ layers in **5** (Fig. 8d). Interestingly, these heptanuclear inorganic core units in **5** may be described as puckered versions of the $\{Cu_7\}$ units observed in siblings **2–4** (Fig. 5 *cf.* Fig. 8d). A single μ-OMe^- ion (*via* O9 and O73 respectively) also aids cage formation within each heptanuclear section while two terminal H_2O ligands (O75 and O76) complete the coordination spheres at centres Cu3, Cu5 and Cu6 respectively (Cu3–O76 = 2.570 Å, Cu5–O76 = 2.515 Å and Cu6–O75 = 2.479 Å). Likewise terminal MeOH moieties partake in the same role at centres labelled Cu2 (Cu2–O74 = 2.544 Å), Cu4 (Cu4–O102 = 2.633 Å), Cu25 (Cu25–O61 = 2.331 Å), Cu26 (Cu26–O73 = 2.484 Å) and Cu28 (Cu26–O73 = 2.545 Å). The two $\{Cu_7\}$ fragments are connected to the $\{Cu_{16}\}$ mainframe through characteristically long Cu–O contacts namely through interactions with the aforementioned μ-bridging OH^- ions at distances of: 2.670 Å (Cu4–O22) and 2.686 Å (Cu27–O45).

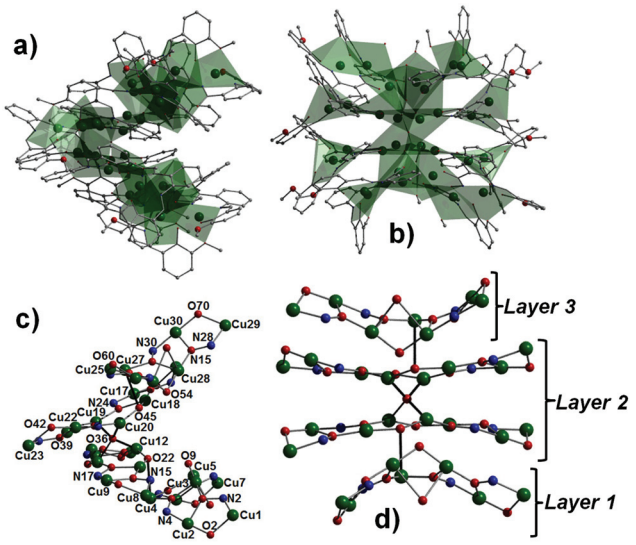

Fig. 8 (a) and (b) Two perspectives of the cluster in **5** as viewed in polyhedral mode. All hydrogen atoms have been omitted for clarity. (c and d) Two perspectives of the inorganic core in **5**. Image d shows the three distinct near planar layers forming the core. The long Cu–O contacts linking the layers are given as thick black lines.

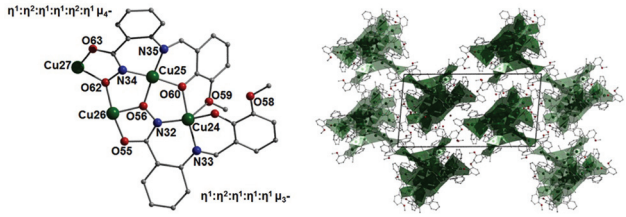

Fig. 9 (left) The two distinct bonding modes exhibited by the L_1^{3-} ligands in $[Cu_{30}]$ (**5**). (right) Packing of the crystals in **5** as viewed along the *a* cell direction. All hydrogen atoms and perchlorate counter anions have been omitted for clarity.

Four of the Cu(II) centres in **5** display distorted octahedral geometry (Cu3, Cu4, Cu27 and Cu28), while the remaining twenty six metal centres exhibit distorted square planar or square based pyramidal geometries. More specifically, the majority of Cu(II) metal centres within the central $\{Cu_{16}\}$ belt exhibit distorted square planar geometries (Cu16 and Cu23 centres are distorted square based pyramidal), while a distorted square based pyramidal geometry dominates within the two $\{Cu_7\}$ moieties in **5** (τ values ranging from 0.017 (Cu26) to 0.298 (Cu1)). Four charge balancing and crystallographically independent ClO_4^- anions lie away from the $[Cu_{30}]$ structure in **5** and are held in position by H-bond interactions with adjacent L_1^{3-} ligand protons (Cl1(O89A)···H360(C360) = 2.655 Å, Cl3(O66)···H40(C40) = 2.646 Å). No obvious intramolecular interactions are observed within the cage in **5**. The $\{Cu_{30}\}$ units arrange in superimposable rows along the *a* unit cell direction and these chains then align using a brickwork pattern along the *bc* plane (Fig. 9-right).

The near planar units within all five complexes (**1–5**) may be described as fragments of metallacrown structures as first highlighted by Pecoraro and co-workers.[18] This is perhaps not surprising as ligands L_1H_3, L_2H_3 and L_3H_3 share similarities with known metallacrown-directing ligands. Moreover, the subsequent linking of our planar units into larger architectures has precedence in metallacrown coordination chemistry.[19] The deviation from planar metallacrown formation in **1–5** is presumably due to ligand driven steric effects. For instance, the puckered sheets diverging away from one another to form the taco-shaped topologies in siblings **1** and **4** and the Pac-Man configuration in **5**.

Unexpected twists

During our synthetic investigations, we inadvertently discovered that by re-dissolving the dried solid obtained from the evaporation of the mother liquor in reactions that produced complex **1** into acetonitrile, an entirely different and un-

expected coordination polymer was produced. More specifically, a methanolic reaction mixture comprising $Cu(ClO_4)_2{\cdot}6H_2O$, 2-(amino)phenylhydroxamic acid and 2-hydroxy-3-methoxybenzaldehyde was evaporated to dryness under reduced pressure and the resultant powder recrystallised from acetonitrile. We initially proposed that the addition of heat along with the solvent removal step would promote the required aldehyde-imine Schiff base coupling. The result was the 1D coordination polymer $\{[Cu(II)(L_4)]{\cdot}H_2O\}_n$ (**6**) comprising the new ligand [[2-[(*E*)-(2-hydroxy-3-methoxy-phenyl)methyleneamino]benzoyl]-amino]ethanimidate (L_4H_2; Fig. 10). This new ligand stems from the Cu(II) mediated addition of a MeCN group at the hydroxyl position of the hydroxamate moiety, thus forming an ethanimidate functionality which upon Cu(II) ligation gives rise to the formation of the pseudo macrocyclic L_4^{2-} ligand in **6** (Fig. 10). Indeed, Tolman *et al.* report the attachment of a MeCN functional group to a pyrazolyl ring *via* a Cu-mediated cycloaddition reaction, resulting in a novel heterocyclic ring system.[20] Complex **6** crystallises in the monoclinic *C*2/*c* space group and all pertinent X-ray diffraction data are given in Table S2.†

The Cu(II) centre (Cu1) displays an almost perfect square based pyramidal geometry with a τ value of 0.016. The equatorial positions at the Cu1 metal centre are occupied by a single chelating L_4^{2-} ligand moiety *via* the phenolic oxygen atom (O2), the imine nitrogen atom (N1), the nitrogen atom of the hydroxamate functional group (N2) and the nitrogen atom of the ethanimidate group (N3), resulting in bond lengths ranging between 1.921 and 1.970 Å. The coordination is completed at the axial position of the Cu1 centre *via* the carbonyl oxygen atom (O3) of a second L_4^{2-} ligand giving a Cu1–O3′ bond length of 2.338 Å. The result is the 1D chain topology in **6** possessing an intra-chain Cu1···Cu1 distance of 5.220 Å. A single water of crystallisation lies near each $\{Cu(L_4)\}$ unit and is locked into position by three hydrogen bonding interactions with aliphatic protons (H3H) and oxygen donor atoms (O1 and O2) of the L_4^{2-} ligands (O5···(H3H)N3 = 2.142 Å, O5(H5A)···O1 = 2.206 Å and O5(H5A)···O2 = 2.303 Å) (Fig. S4†). These waters of crystallisation also partake in H-bonding throughout the crystal structure in **6** (O5···(H5B′)O5′ = 2.151 Å). The individual 1D rows in **6** propagate along the *b* axis of the unit cell in a superimposable manner and these rows then pack into a common brickwork motif (Fig. S5†).

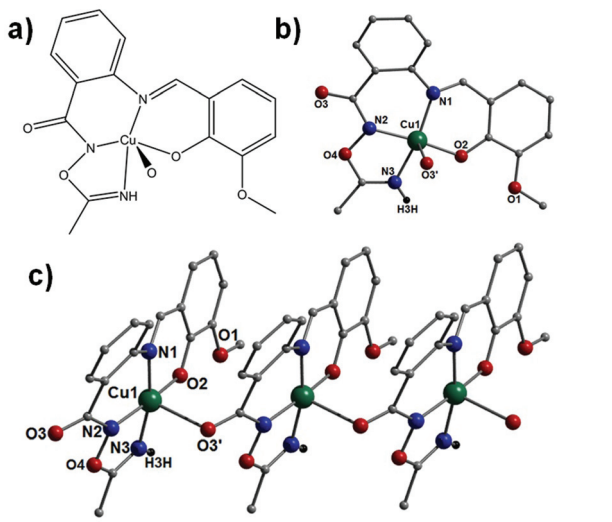

Fig. 10 (a) ChemDraw representation and crystal structure (b) of one $[Cu(II)(L_4)]$ unit in **6** including the next bridging oxygen (O3′) atom. (c) Representation of the repeating 1D structure in **6** (comprising three $[Cu(II)(L_4)]$ units). The majority of hydrogen atoms and all H_2O solvents of crystallisation were omitted for clarity.

Magnetic susceptibility studies

As described previously and illustrated in Fig. S6,† the molecular structure in **1**, **2**, **4** and **5** contain linked polynuclear layers of either $\{Cu_5\}$ (in **1**) or $\{Cu_7\}$ (in **2**, **4** and **5**) units, whose structures may also be described as comprising edge- and vertex sharing $\{Cu(II)_3\}$ triangular sub-units. Moreover, these individual polymetallic layers are connected by long axial Cu–O contacts *via* filled Cu(II) d_{z^2} orbitals. We can therefore envisage antiferromagnetic exchange within the layers and negligible magnetic interactions between layers. In this scenario, the layers of odd numbered Cu(II) ions would likely lead to small but magnetic ground states. Magnetic data support such an hypothesis. Dc magnetic susceptibility measurements were performed on powdered microcrystalline samples of **1**, **2**, **4** and **5** in the 300–5 K temperature range in an applied field of 0.1 T (Fig. 11). The room temperature $\chi_M T$ values of 2.41 (**1**), 3.53 (**2**) 3.79 (**4**) and 11.6 (**5**) $cm^3\ K\ mol^{-1}$ are well below their expected spin-only values of ~4.13 (**1**), 5.78 (**2** and **4**) and 12.4 (**5**) $cm^3\ K\ mol^{-1}$ (assuming g = 2.1) and are indicative of strong intramolecular antiferromagnetic exchange between the Cu(II) ions within the layers of each complex. The $\chi_M T$ *vs.* T plot for **1** shows a steady drop in its magnetic susceptibility

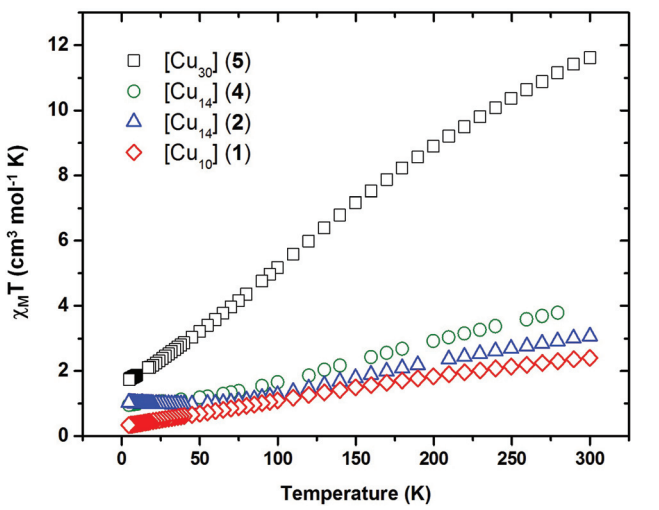

Fig. 11 Plots of $\chi_M T$ *vs.* T for complex **1**, **2**, **4** and **5**.

product which becomes a little more abrupt below 50 K, before reaching a value of 0.34 cm^3 mol^{-1} K at 5 K. Likewise, [Cu_{14}] complexes **2** and **4** exhibit a gradual decline in their $\chi_M T$ products before reaching T = 5 K values of 0.96 and 1.03 cm^3 mol^{-1} K, respectively (Fig. 11). A much more rapid decline in the magnetic susceptibility of complex **5** is shown along the entire temperature range, giving a 5 K value of 1.73 cm^3 K mol^{-1}. Despite our efforts, the complexity of the magnetic cores in these complexes, which contain multiple different exchange interaction pathways, precludes any quantitative analysis of the data.

Conclusions

The Schiff base condensation of precursors 2-(amino)phenylhydroxamic acid and 2-hydroxy-3-methoxybenzaldehyde, 5-bromo-2-hydroxy-3-methoxybenzaldehyde or 2-hydroxybenzaldehyde in the presence of Cu(II) ions leads to the *in situ* formation and subsequent metal ligation of the polydentate ligands *o*-[(*E*)-(2-hydroxy-3-methoxyphenyl)methylideneamino]-benzohydroxamic acid (L_1H_3), *o*-[(*E*)-(2-hydroxy-3-methoxy-5-bromophenyl)methylideneamino]benzohydroxamic acid (L_2H_3) and *o*-[(*E*)-(*o*-2-hydroxyphenyl)methylideneamino]benzohydroxamic acid (L_3H_3), respectively. The end products, depending on specific reaction conditions, are the Cu(II) cages: $[Cu(II)_{10}(L_1)_4(2\text{-aph})_2(H_2O)_2](ClO_4)_4\cdot 5MeOH$ (**1**), $[Cu(II)_{14}(L_1)_8(MeOH)_{2.5}(H_2O)_{7.5}](NO_3)_4\cdot 3MeOH\cdot 7H_2O$ (**2**), $[Cu(II)_{14}(L_2)_8(MeOH)_4(H_2O)_6](NO_3)_4\cdot 6H_2O$ (**3**), $[Cu(II)_{14}(L_3)_8(MeOH)_6(H_2O)_2](NO_3)_4\cdot 4MeOH\cdot 8H_2O$ (**4**) and $[Cu(II)_{30}O(OH)_4(OMe)_2(L_1)_{16}(MeOH)_4(H_2O)_2](ClO_4)_4\cdot 2MeOH\cdot 30H_2O$ (**5**). The introduction of acetonitrile into the synthesis of **1** results in the *in situ* Cu(II) mediated formation of the unexpected ligand [[2-[(*E*)-(2-hydroxy-3-methoxy-phenyl)methyleneamino]benzoyl]amino]-ethanimidate (L_4H_2) and this ligand modification gives rise to the formation of the 1D coordination polymer $\{[Cu(II)(L_4)]\cdot H_2O\}_n$(**6**). Dc magnetic susceptibility studies on complexes **1**, **2**, **4** and **5** indicate strong antiferromagnetic exchange between nearest neighbours resulting in small, but magnetic ground states within the Cu layers and negligible inter-layer interactions in all cases. In this work, we have employed an elegant synthon previously used in the field of subcomponent self-assembly to drive the *in situ* formation of ligands comprising multiple metal binding sites to aid the growth of large paramagnetic cages. Work is currently underway on probing further the coordination ability of these interesting ligands with other paramagnetic metal ions. We are also currently investigating these ligands towards metal sequestration.

Experimental

Infra-red spectra were recorded on a Perkin Elmer FT-IR Spectrum One spectrometer equipped with a Universal ATR Sampling accessory (NUI Galway). Elemental analysis was carried out at the School of Chemistry microanalysis service, NUI Galway. Variable-temperature, solid-state direct current (dc) magnetic susceptibility data down to 5 K were collected on a Quantum Design MPMS-XL SQUID magnetometer equipped with a 7 T dc magnet. Diamagnetic corrections were applied to the observed paramagnetic susceptibilities using Pascal's constants. All measured complexes were set in eicosane to avoid torqueing of the crystallites. All magnetic samples are collected as single-crystalline products and analysed using microanalysis and IR measurements prior to their magnetic assessment. If necessary, phase purity between cross-batches are validated using unit cell checks and IR measurements.

Crystallography

The X-ray data for crystal structures of **1–6** were collected on an Xcalibur S single crystal diffractometer (Oxford Diffraction) using an enhanced Mo source (CCDC numbers: 1055293–1055298). Each data reduction was carried out on the CrysAlisPro software package. The crystal structures were solved by direct methods (SHELXS-97)[21] and refined by full matrix least squares using SHELXL-97.[21] SHELX operations were automated using the OSCAIL software package,[22] except for crystal structures **2** and **3**, where the SHELX-2013[23] within the OLEX2[24] suite was employed. All hydrogen atoms in **1–6** were assigned to calculated positions.

The unbound perchlorate in **1** (Cl2–O12–O15) was modelled as disordered over two sites and restrained using the DFIX command. The carbon atom, C1, belonging to a methoxide group on an L_1^{3-} unit, was modelled as disordered over two sites (70 : 30). Residual electron density in solvent accessible voids and channels were observed in **1** that required modelled using the SQUEEZE program.[25] The four voids in **1** represented a total volume of 1720 $Å^3$, which equates to five MeOH solvent molecules of crystallisation per [Cu_{14}] cage (commensurate with microanalysis results on **1**; calculated formula: **1**·5MeOH *cf.* elemental analysis: **1**·5MeOH).

In the crystal structure of **2**, four NO_3^- anions have been assigned. The nitrate labelled N17–O47–O49 is disordered and modelled over two sites with a 70 : 30 ratio. The NO_3^- moiety labelled N18–O50–O52 has been refined as fully occupied with displacement parameters refined as isotropic only. The remaining two nitrates have been split over two sites with partial occupancies arbitrarily set at half. Moreover, the atom O60A forms part of a partially occupied NO_3^- anion (N20A–O60A–O61A–O62A), which shares the same site as a partially occupied water (O11) at Cu1. Likewise, the Cu6 centre is bound to a 50 : 50 partial occupancy comprising a NO_3^- anion (N20B–O60B–O61B–O62B) and a MeOH (C201–O60C) ligand. Several DFIX/DANG restraints were used to maintain sensible geometry with respect to the disordered $NO_3^-$and MeOH ligands in **2**, while SIMU/DELU restraints were used to model displacement parameters. More specifically, the EAPD restraints were applied to atoms O60A–O62A, O60B–O602B, O60C and O47A/O47B. The crystal structure in **2** contains a large number of disordered, uncoordinated solvent molecules (H_2O/MeOH) located in the voids. A number of them have been successfully assigned (some as half occupied and isotropic only). The remaining highly diffused electron density

(negligible amount) was removed using SMTBX algorithms within the OLEX2 suite, which improves the final model and led structure refinement to convergence. Elemental analysis on **2** support these residual electron density calculations although solvent loss was observed upon drying (calculated formula: **2**·3MeOH·7H_2O *cf.* elemental analysis: **2**·5H_2O).

Significant disorder in **3** was observed at Cu5 and was therefore modelled at 50% occupancy along with the bound L_2^{3-} atoms C86–C92A. DFIX, DANG and SIMU restraints were also employed. All disorder was modelled as anisotropic where possible; however O73A/B and O103 required to remain isotropic. The SMTBX function was employed to treat diffuse solvent and the NO_3^- counter anions in **3**. The SQUEEZE program was required to account for the residual electron density within the two independent accessible voids in **3** (total void volume = 740 Å^3) and was assumed to contain six waters of crystallisation per cage (commensurate with microanalysis results on **3**; calculated formula: **3**·6H_2O *cf.* elemental analysis: **3**·6H_2O).

All non-hydrogen atoms in **4** were refined as anisotropic with the exception of one NO_3^- anion (N10–O17–19), which has been refined as isotropic. A DFIX restraint was also required for this anion. All solvent molecules of crystallisation located in the lattice also remained isotropic. DFIX restraints were used for MeOH solvents of crystallisation in complex **4** (C71–O42, C72–O41 and C73–O44). The SQUEEZE program was required to account for the residual electron density within the four independent accessible voids in **4** (total void volume = 360 Å^3) and was assumed to contain four waters of crystallisation per cage (commensurate with microanalysis results on **4**; calculated formula: **4**·4MeOH·8H_2O *cf.* elemental analysis: **4**·4MeOH·4H_2O).

Despite carrying out numerous collections, weak X-ray data was obtained from all crystals of complex **5** (R_{int} = 0.1034, wR_2 = 0.3398 as given in this work). All C atoms required remaining isotropic and all H atoms were placed in calculated positions. Residual electron density in solvent accessible voids and channels were observed in **5** and so were modelled using the SQUEEZE program.[25] The three channels in **5** (total voids volume ~1995 Å^3) contained extremely diffuse electron density and were assumed to contain numerous methanol and waters of crystallisation. CHN analysis on **5** supported these observations although significant solvent loss was observed upon drying (calculated formula: **5**·2MeOH·30H_2O *cf.* elemental analysis: **5**·11H_2O).

Preparation of complexes

All reactions were performed under aerobic conditions and all reagents and solvents were used as purchased. *Caution*: Although no problems were encountered in this work, care should be taken when manipulating the potentially explosive perchlorate and nitrate salts. 2-(Amino)phenylhydroxamic acid was synthesised using previously reported synthetic procedures.[26] The solvothermal synthesis of **5** was carried out in a Hereaus (UT6420-Thermo Scientific) oven using spring loaded stainless steel digestion vessels (23 cm^3 capacity) produced by the Parr Instrument Company. The microwave synthesis of **2** was carried in a CEM Discover® microwave reactor.

$[Cu(II)_{10}(L_1)_4(2\text{-aph})_2(H_2O)_2](ClO_4)_4$·5MeOH (1). $Cu(ClO_4)_2$·6H_2O (0.25 g, 0.68 mmol), 2-(amino)phenylhydroxamic acid (0.052 g, 0.34 mmol), 2-hydroxy-3-methoxybenzaldehyde (0.052 g, 0.34 mmol) and NaOH (0.027 g, 0.68 mmol) were dissolved in 30 cm^3 of MeOH and stirred for 4 h. The resultant dark green solution was then filtered and aliquots of the mother liquid were then diffused with diethyl ether. Dark green X-ray quality crystals of **1** began to form after two days. The crystals were collected and air dried to give a yield of approximately 5%. FT-IR (cm^{-1}): 2937(w), 1605(m), 1580(m), 1543(m), 1490(w), 1433(m), 1373(m), 1298(w), 1234(m), 1183(m), 1160(w), 1078(s), 977(w), 932(m), 871(w), 853(w), 771(m), 740(m), 687(m), 651(w), 621(s), 579(m), 556(m), 536(m), 524(m), 519(s). Elemental analysis (%) calculated (found) for $C_{79}H_{80}Cl_4N_{12}O_{43}Cu_{10}$ (**1**·5MeOH): C 35.63 (35.27), H 3.03 (2.89), N 6.31 (6.59).

$[Cu(II)_{14}(L_1)_8(MeOH)_{2.5}(H_2O)_{7.5}](NO_3)_4$·3MeOH·7$H_2O$ (2). *Method A*: $Cu(NO_3)_2$·3H_2O (0.25 g, 1.04 mmol), 2-(amino)-phenylhydroxamic acid (0.08 g, 0.53 mmol), 2-hydroxy-3-methoxybenzaldehyde (0.08 g, 0.53 mmol) and NaOH (0.042 g, 1.04 mmol) were dissolved in 30 cm^3 of MeOH and stirred for 4 h. The resultant dark green solution was then filtered and X-ray quality crystals of **2** began to form after two days. *Method B*: $Cu(NO_3)_2$·3H_2O (0.25 g, 1.04 mmol), 2-(amino)phenylhydroxamic acid (0.08 g, 0.53 mmol), 2-hydroxy-3-methoxybenzaldehyde (0.08 g, 0.53 mmol) and NaOH (0.042 g, 1.04 mmol) were dissolved in 15 cm^3 of MeOH in a microwave reactor vial which was stirred for 2 minutes. The glass vial was then sealed and inserted into a microwave oven reactor. The reaction was maintained at T = 110 °C, pressure = 110 psi and power = 200 W for a total of 5 min. The resultant green solution was left to cool before filtration and slow evaporation of the mother liquor gave X-ray quality crystals of **2** after two days. Both synthetic methodologies gave approximately 10% yields. FT-IR (cm^{-1}): 3065(w), 1607(w), 1581(m), 1541(m), 1490(w), 1457(w), 1432(m), 1372(m), 1328(m), 1233(m), 1183(m), 1100(m), 1080(w), 1027(w), 979(m), 932(m), 871(w), 854(m), 827(w), 786(m), 772(m), 740(s), 689(m), 652(m), 625(m), 586(m), 555(m), 535(m), 524(s). Elemental analysis (%) calculated (found) for $C_{123}H_{126}N_{20}O_{60}Cu_{14}$ (**2**·5H_2O): C 39.56 (39.18), H 3.40 (2.96), N 7.50 (7.30).

$[Cu(II)_{14}(L_2)_8(MeOH)_4(H_2O)_6](NO_3)_4$·6$H_2O$ (3). $Cu(NO_3)_2$·3H_2O (0.25 g, 1.04 mmol) was added to a 30 cm^3 methanolic solution of 2-amino-phenylhydroxamic acid (0.078 g, 0.52 mmol) and 5-bromo-2-hydroxy-3-methoxybenzaldehyde (0.12 g, 0.52 mmol) and stirred for approximately 2 minutes. The solution became very dark green in colour. NaOH (0.04 g, 1.03 mmol) was then added and the solution stirred for a further 4 hours. The resultant solution was then filtered and X-ray quality crystals of **3** were obtained after 1 week in 15% yield. FT-IR (cm^{-1}): 3400(w), 29 323(w), 2427(w), 1606(w), 1583(s), 1547(s), 1489(m), 1436(w), 1384(s), 1328(w), 1293(w), 1241(s), 1184(m), 1159(w), 1120(w), 1100(m), 1031(m), 980(m), 934(m), 881(w), 866(w), 841(w), 795(m), 770(w), 758(w), 720(m),

688(w), 665(w), 633(w), 5669(m), 451(m). Elemental analysis (%) calculated (found) for $C_{124}H_{120}N_{20}O_{60}Br_8Cu_{14}$ (**3**·6H_2O): C 34.01 (34.18), H 2.76 (2.52), N 6.40 (5.98).

$[Cu(II)_{14}(L_3)_8(MeOH)_6(H_2O)_2](NO_3)_4$·4MeOH·8$H_2O$ (4). Cu$(NO_3)_2$·3H_2O (0.25 g, 1.04 mmol), 2-(amino)phenylhydroxamic acid (0.08 g, 0.53 mmol), salicyaldehyde (0.058 cm^3, 0.53 mmol) and NaOH (0.042 g, 1.04 mmol) were dissolved in 30 cm^3 of MeOH and stirred for 4 h. The resultant dark green solution was filtered and X-ray quality crystals of **4** were obtained from both slow evaporation and diethyl ether diffusion (total yield = 10%). FT-IR (cm^{-1}): 3404(w), 3075(w), 1607(m), 1578(m), 1543(m), 1486(m), 1463(m), 1434(m), 1373(m), 1328(m), 1284(s), 1228(m), 1184(m), 1152(m), 1099(s), 1029(w), 987(m), 930(m), 863(m), 806(m), 753(s), 740(s), 679(s). Elemental analysis (%) calculated (found) as $C_{122}H_{124}N_{20}O_{56}Cu_{14}$ (**4**·4MeOH·4H_2O): C 40.08 (40.09), H 3.42 (3.83), N 7.66 (7.30).

$[Cu(II)_{30}(O)_1(OH)_4(OMe)_2(L_1)_{16}(MeOH)_4(H_2O)_2](ClO_4)_4$·2MeOH·30$H_2O$ (5). $Cu(ClO_4)_2$·6H_2O (0.1 g, 0.27 mmol), 2-(amino)phenylhydroxamic acid (0.021 g, 0.14 mmol), 2-hydroxy-3-methoxybenzaldehyde (0.021 g, 0.14 mmol) and NEt_4(OH) (0.7 cm^3, 0.72 g, 4.89 mmol) were dissolved in 10 cm^3 of MeOH and stirred for 1 h. The resultant dark green solution was then placed in a teflon lined stainless steel autoclave and heated at 100 °C for 24 h followed by slow cooling over a further 24 h period. Dark green X-ray quality crystals of **5** were collected in 5% yield. FT-IR (cm^{-1}): 3387(w), 1605(m), 1579(m), 1540(m), 1488(w), 1432(m), 1374(m), 1297(w), 1233(m), 1184(m), 1093(s), 978(m), 947(m), 853(w), 771(m), 737(s), 687(m), 651(m), 623(s), 557(m), 531(m), 524(m). Elemental analysis (%) calculated (found) for $C_{246}H_{228}N_{32}O_{104}Cl_4Cu_{30}$ (**5**·11H_2O): C 40.23 (39.94), H 3.13 (2.85), N 6.10 (6.59).

{$[Cu(II)(L_4)]$·H_2O}$_n$ (6). $Cu(ClO_4)_2$·6H_2O (0.25 g, 0.68 mmol), L_4H_2 (0.104 g, 0.68 mmol) and 2-hydroxy-3-methoxybenzaldehyde (0.104 g, 0.68 mmol) were dissolved in 30 cm^3 of MeOH and stirred for 5 min. NaOMe (0.073 g, 1.36 mmol) was added to the solution. The dark green solution was then stirred overnight (16 h), after which the solvent was removed under reduced pressure and the green solid re-dissolved in 20 cm^3 of MeCN and stirred for a further 1 h. This solution was then filtered and left to slowly evaporate for a few days, resulting in the formation of dark green X-ray quality crystals of **6** in 20% yield. FT-IR (cm^{-1}): 3428(w), 3347(w), 3061(w), 1673(w), 1583(s), 1559(m), 1530(m), 1447(s), 1391(m), 1349(m), 1234(s), 1183(s), 1143(m), 1108(m), 1078(m), 1025(w), 1009(m), 985(m), 940(m), 899(w), 877(m), 860(m), 836(m), 771(m), 735(s), 700(s). Elemental analysis (%) calculated (found) for $C_{17}H_{15}N_3O_4Cu_1$ (**6**): C 52.51 (52.16), H 3.89 (3.88), N 10.81 (10.41).

Acknowledgements

LFJ would like to thank the College of Science, NUI Galway (CM), the School of Chemistry, Bangor University (DWW) and the EPSRC (National Crystallographic Service) for their support.

Notes and references

1 T. K. Ronson, S. Zarra, S. P. Black and J. R. Nitschke, *Chem. Commun.*, 2013, **49**, 2476–2490.
2 C. D. Meyer, C. S. Joiner and J. F. Stoddart, *Chem. Soc. Rev.*, 2007, **36**, 1705–1723.
3 (*a*) X.-P. Zhou, Y. Wu and D. Li, *J. Am. Chem. Soc.*, 2013, **135**, 16062–16065; (*b*) X.-P. Zhou, J. Liu, S.-Z. Zhan, J.-R. Yang, D. Li, K.-M. Ng, R. W.-Y. Sun and C.-M. Che, *J. Am. Chem. Soc.*, 2012, **134**, 8042–8045; (*c*) S. Yi, V. Brega, B. Captain and A. E. Kaifer, *Chem. Commun.*, 2012, **48**, 10295–10297; (*d*) H. Bunzen, Nonappa, E. Kalenius, S. Hietala and E. Kolehmainen, *Chem. – Eur. J.*, 2013, **19**, 12978–12981.
4 (*a*) P. P. Neelakandan, A. Jimenez and J. R. Nitschke, *Chem. Sci.*, 2014, **5**, 908–915; (*b*) J. Mosquera, S. Zarra and J. R. Nitschke, *Angew. Chem., Int. Ed.*, 2014, **53**, 1556–1559.
5 M. U. Anwar, Y. Lan, L. M. C. Beltran, R. Clerac, S. Pfirrmann, C. E. Anson and A. K. Powell, *Inorg. Chem.*, 2009, **48**, 5177–5186.
6 D. R. Turner, S. N. Pek, J. D. Cashion, B. Moubaraki, K. S. Murray and S. R. Batten, *Dalton Trans.*, 2008, 6877–6879.
7 A. S. R. Chesman, D. R. Turner, B. Moubaraki, K. S. Murray, G. B. Deacon and S. R. Batten, *Dalton Trans.*, 2012, **41**, 3751–3757.
8 (*a*) C. McDonald, S. Sanz, E. K. Brechin, M. K. Singh, G. Rajaraman, D. Gaynor and L. F. Jones, *RSC Adv.*, 2014, **4** (72), 38182–38191; (*b*) C. McDonald, T. Whyte, S. M. Taylor, S. Sanz, E. K. Brechin, D. Gaynor and L. F. Jones, *CrystEngComm*, 2013, **15**(34), 6672–6681.
9 (*a*) S. T. Meally, C. McDonald, P. Kealy, S. M. Taylor, E. K. Brechin and L. F. Jones, *Dalton Trans.*, 2012, **41**(18), 5610–5616; (*b*) S. T. Meally, C. McDonald, G. Karotsis, G. S. Papaefstathiou, E. K. Brechin, P. W. Dunne, P. McArdle, N. P. Power and L. F. Jones, *Dalton Trans.*, 2010, **39**, 4809–4816; (*c*) S. T. Meally, G. Karotsis, E. K. Brechin, G. S. Papaefstathiou, P. W. Dunne, P. McArdle and L. F. Jones, *CrystEngComm*, 2010, **12**, 59–63.
10 (*a*) G. L. Abbati, A. Caneschi, A. Cornia, A. C. Fabretti, Y. A. Pozdniakova and O. I. Shchegolikhina, *Angew. Chem., Int. Ed.*, 2002, **41**, 4517–4520; (*b*) T. Kajiwara, N. Kon, S. Yokozawa, T. Ito, N. Iki and S. Miyano, *J. Am. Chem. Soc.*, 2002, **124**, 11274–11275; (*c*) V. Chandrasekhar, L. Nagarajan, K. Gopal, V. Baskar and P. Kögerler, *Dalton Trans.*, 2005, 3143–3145; (*d*) F. Pan, J. Wu, H. Hou and Y. Fan, *Cryst. Growth Des.*, 2010, **10**, 3835–3837; (*e*) V. Chandrasekhar, L. Nagarajan, S. Hossain, K. Gopal, S. Ghosh and S. Verma, *Inorg. Chem.*, 2012, **51**, 5605–5616.
11 (*a*) C.-H. Chang, K. C. Hwang, C.-S. Liu, Y. Chi, A. J. Carty, L. Scoles, S.-M. Peng, G.-H. Lee and J. Reedjik, *Angew. Chem., Int. Ed.*, 2001, **40**, 4651–4653; (*b*) G. C. Vlahopoulou, T. C. Stamatatos, V. Psycharis, S. P. Perlepes and G. Christou, *Dalton Trans.*, 2009, 3646–3649.
12 (*a*) P. J. M. W. L. Birker and H. C. Freeman, *J. Am. Chem. Soc.*, 1977, 6890–6899; (*b*) P. J. M. W. L. Birker, *Inorg.*

Chem., 1979, **18**(12), 3502–3506; (*c*) H. J. Schugar, C.-C. Ou, J. A. Thich, J. A. Potenza, T. R. Felthouse, M. S. Haddad, D. N. Hendrickson, W. Furey Jr. and R. A. Lalancette, *Inorg. Chem.*, 1980, **19**, 543–552; (*d*) A. Mukherjee, M. Nethaji and A. R. Chakravarty, *Angew. Chem., Int. Ed.*, 2004, **43**, 87–90; (*e*) M. B. Duriska, S. M. Neville, J. Lu, S. S. Iremonger, J. F. Boas, C. J. Kepert and S. R. Batten, *Angew. Chem., Int. Ed.*, 2009, **48**, 8919–8922.

13 C. Xu, X.-Y. Yi, T.-K. Duan, Q. Chen and Q.-F. Zhang, *Polyhedron*, 2011, **30**, 2637–2643.

14 For examples see: (*a*) S. Dehnen and D. Fenske, *Chem. – Eur. J.*, 1996, **2**(11), 1407–1416; (*b*) N. Zhu and D. Fenske, *J. Chem. Soc., Dalton Trans.*, 1999, 1067–1075; (*c*) M. W. DeGroot, M. W. Cockburn, M. S. Workentin and J. F. Corrigan, *Inorg. Chem.*, 2001, **40**, 4678–4685; (*d*) O. Fuhr, L. Fernandez-Recio and D. Fenske, *Eur. J. Inorg. Chem.*, 2005, 2306–2314; (*e*) E. A. Turner, Y. Huang and J. F. Corrigan, *Z. Anorg. Allg. Chem.*, 2007, **633**, 2135–2137.

15 M.-L. Fu, I. Issac, D. Fenske and O. Fuhr, *Angew. Chem., Int. Ed.*, 2010, **49**, 6899–6903.

16 M. Murugesu, R. Clerac, C. E. Anson and A. K. Powell, *Chem. Commun.*, 2004, 1598–1599.

17 M. Murugesu, R. Clerac, C. E. Anson and A. K. Powell, *Inorg. Chem.*, 2004, **43**, 7269–7271.

18 For an extensive review on metallacrowns see: G. Mezei, C. M. Zaleski and V. L. Pecoraro, *Chem. Rev.*, 2007, **107**, 4933–5003.

19 G. Psomas, C. Dendrinou-Samara, M. Alexiou, A. Tsohos, C. P. Raptopoulou, A. Terzis and D. P. Kessissoglou, *Inorg. Chem.*, 1998, **37**, 6556–6557.

20 J. L. Schneider, V. G. Young Jr. and W. B. Tolman, *Inorg. Chem.*, 2001, **40**, 165–168.

21 (*a*) G. M. Sheldrick, *Acta. Crystallogr., Sect. A: Fundam. Crystallogr.*, 1990, **46**, 467; (*b*) G. M. Sheldrick, *SHELXL-97, A computer programme for crystal structure determination*, University of Gottingen, 1997.

22 P. McArdle, P. Daly and D. Cunningham, *J. Appl. Crystallogr.*, 2002, **35**, 378.

23 G. M. Sheldrick, *Acta. Crystallogr., Sect. A: Fundam. Crystallogr.*, 2008, **64**, 112.

24 O. V. Dolomanov, L. J. Bourhis, R. J. Gildea, J. A. K. Howard and H. Puschmann, *J. Appl. Crystallogr.*, 2009, **42**, 339–341.

25 (*a*) A. Spek, *J. Appl. Crystallogr.*, 2003, **36**, 7–13; (*b*) P. van der Sluis and A. L. Spek, *Acta Crystallogr., Sect. A: Fundam. Crystallogr.*, 1990, **46**, 194–201.

26 D. Gaynor, Z. A. Starikova, W. Haase and K. B. Nolan, *Dalton Trans.*, 2001, 1578.